COMMUNICATION

Fuel Cells

ADVANCED
ENERGY
MATERIALS

www.advenergymat.d

Check for
updates

Atomic Fe-Doped MOF-Derived Carbon Polyhedrons with High Active-Center Density and Ultra-High Performance toward PEM Fuel Cells

Yijie Deng, Bin Chi, Jing Li, Guanghua Wang, Long Zheng, Xiudong Shi, Zhiming Cui, Li Du,* Shijun Liao,* Ketao Zang, Jun Luo, Yongfeng Hu, and Xueliang Sun

A metalorganic gaseous doping approach for constructing nitrogen-doped carbon polyhedron catalysts embedded with single Fe atoms is reported. The resulting catalysts are characterized using scanning transmission electron microscopy, X-ray photoelectron spectroscopy, and X-ray absorption spectroscopy; for the optimal sample, calculated densities of Fe–N_x sites and active N sites reach 1.75812×10^{13} and 1.93693×10^{14} sites cm^{-2}, respectively. Its oxygen reduction reaction half-wave potential (0.864 V) is 50 mV higher than that of 20 wt% Pt/C catalyst in an alkaline medium and comparable to the latter (0.78 V vs 0.84 V) in an acidic medium, along with outstanding durability. More importantly, when used as a hydrogen–oxygen polymer electrolyte membrane fuel cell (PEMFC) cathode catalyst with a catalyst loading as low as 1 mg cm^{-2} (compared with a conventional loading of 4 mg cm^{-2}), it exhibits a current density of 1100 mA cm^{-2} at 0.6 V and 637 mA cm^{-2} at 0.7 V, with a power density of 775 mW cm^{-2}, or 0.775 kW g^{-1} of catalyst. In a hydrogen–air PEMFC, current density reaches 650 mA cm^{-2} at 0.6 V and 350 mA cm^{-2} at 0.7 V, and the maximum power density is 463 mW cm^{-2}, which makes it a promising candidate for cathode catalyst toward high-performance PEMFCs.

Dr. Y. J. Deng, Dr. B. Chi, Dr. J. Li, Dr. G. H. Wang, L. Zheng, Dr. X. D. Shi, Prof. Z. M. Cui, Prof. L. Du, Prof. S. J. Liao
The Key Laboratory of Fuel Cell Technology of Guangdong Province
School of Chemistry and Chemical Engineering
South China University of Technology
Guangzhou 510641, China
E-mail: duli@scut.edu.cn; chsjliao@scut.edu.cn
K. Zang, Prof. J. Luo
Center for Electron Microscopy
TUT-FEI Joint Laboratory
Tianjin Key Laboratory of Advanced Functional Porous Materials
Institute for New Energy Materials & Low-Carbon Technologies
School of Materials Science and Engineering
Tianjin University of Technology
Tianjin 300384, China
Dr. Y. F. Hu
Canadian Light Source
44 Innovation Boulevard, Saskatoon, SK S7N 2V3, Canada
Prof. X. L. Sun
Department of Mechanical and Materials Engineering
University of Western Ontario
1151 Richmond St., London, Ontario N6A 3K7, Canada

For the quick development and initial commercialization of proton exchange membrane fuel cells (PEMFCs), one of the serious challenges is the use of scarce, costly platinum as a catalyst to overcome the sluggish kinetics and high overpotential of the oxygen reduction reaction (ORR) at the cathode[1–3] In the last decade, tremendous efforts have been made to explore highly efficient non-precious-metal catalysts, such as doped carbon, to replace Pt/C.[4,5] Single-atom Fe-embedded nitrogen-doped carbon (Fe–N_x/C) has attracted particular attention recently, showing superior ORR performance that makes it a promising material for further investigation[6–11] Though great progress has already been achieved, the rational design and preparation of a single-atom Fe-doped catalyst (Fe–N_x/C) with a large surface area, beneficial porous structure, high active-site density, and high performance in an acidic PEMFC remains a considerable hurdle.[12–15]

Zeolitic imidazole frameworks (ZIFs) are self-assembling, ordered, porous materials with bridging metal atoms and N-containing ligands. ZIFs provide a good platform for the preparation of high-performance carbon catalysts doped with single metal atoms[16,17] Several groups have reported preparing carbon catalysts doped with single Fe (or other metal) atoms using ZIFs or other metal–organic frameworks (MOFs) as precursors[18] For instance, Jiang and co-workers[19] used a porphyrinic MOF as the precursor to prepare single-atom Fe-implanted N-doped porous carbon via a mixed-ligand strategy; their catalyst exhibited excellent oxygen reduction activity in an acidic medium, with a half-wave potential of 0.776 V. Gao and co-workers[20] reported creating a ZIF-derived catalyst doped with N-coordinated single-atom Fe, using a ferrocene encapsulated in ZIF-8 strategy whereby ferrocene was introduced during the assembly of Zn^{2+} ions with 2-methylimidazole; the catalyst exhibited good oxygen reduction activity in an alkaline medium. However, it is still a great challenge for obtaining satisfactory performance in a single acidic PEMFC.
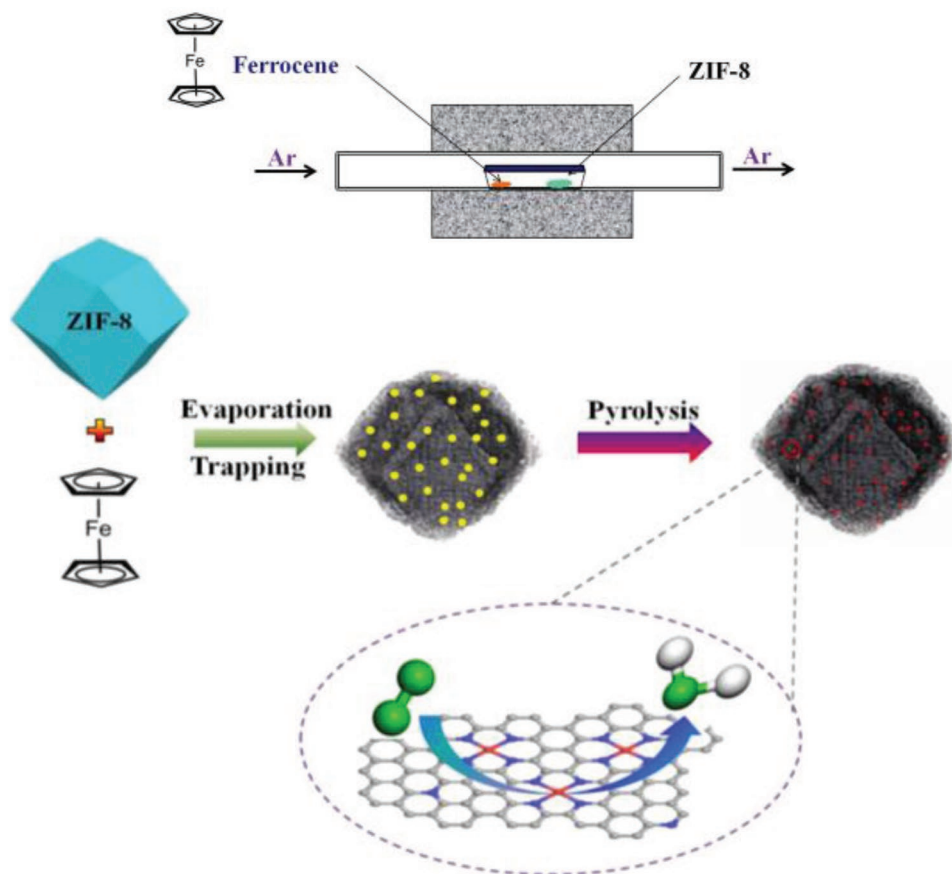
To date, few intensive investigations of single Fe-doped carbon as the cathode catalyst in single PEMFCs have been reported[14,19] Generally, the inadequate performance of doped-carbon

**Scheme 1.** Schematic illustration of preparation of sample.

catalysts in PEMFCs is ascribed primarily to their low active-site density and unfavorable pore structure. In addition, as the usual doped-carbon catalyst loading is about 4 mg cm^{-2}, the resulting cathode catalyst layer is much thicker than that of a commercial Pt/C catalyst (0.2–0.8 mg cm^{-2}), making water and heat management in the fuel cell more difficult[21] Hence, research into achieving high active-site density and optimal porous structure is highly desirable to boost the practical application of doped-carbon catalysts.[22]

Based on above understanding, in the present work, we suggested a novel metallorganic gaseous doping strategy, and prepared a MOF-derived doped-carbon catalyst with high density of active sites/single Fe atoms, well-defined polyhydron morphology, well-balanced porous structure, and high surface area, by the strategy, in which an evaporable iron organic compound, ferrocene are first vaporized, then trapped into ZIF-8 precursors. Amazingly, the catalyst exhibits distinguished enhanced ORR activity and long-term durability in both acidic and alkaline solutions, and its groundbreaking cathode performance in acidic PEMFCs (fed with hydrogen and either oxygen or air) is comparable to that of Pt/C, placing it at the forefront of all reported doped-carbon catalysts.

The ZIF-8 nanocrystals were synthesized by a method described in the literature; the X-ray diffraction (XRD) pattern of the sample suggested the successful synthesis of ZIF-8 (Figures S1 and S3, Supporting Information).[23] The catalysts

were prepared by a metalorganic gaseous doping approach developed by our group, in which ferrocene molecules are first vaporized, then trapped by ZIF-8. As temperature rose up to 950 °C, adsorbed ferrocene species and organic skeleton of ZIF-8 were pyrolysed, and ZIF-8 transformed into porous carbon nanoframe and ferrocene transformed into single atom Fe which further coordinated with N on carbon skeleton. The preparation process is illustrated in **Scheme 1**.[24–26] We tuned and optimized the ratio of ferrocene to ZIF-8 by adjusting the amount of ferrocene.

Figure 1 shows the SEM/TEM images of synthesized C-ZIF-8 and three catalyst samples prepared with various recipe mass ratios of ferrocene to ZIF-8, as well as scanning transmission electron microscopy (STEM) images of C-FeZIF-1.44-950. As shown in Figure 1a–c, all three samples well retained the morphology of ZIF-8 precursor. Compared to the smooth surface of C-ZIF-8-950 (see Figure 1a), the surface of the Fe-doped polyhedrons became rougher as the mass ratio of ferrocene to ZIF-8 increased, which is attributable to the formation of mesopores on the surface. For the sample C-FeZIF-4.44-950, prepared with a mass ratio of ferrocene to ZIF-8 of 4.44, still retained most of the polyhedrons' morphology/structure (Figure 1d), demonstrating that our gaseous doping process is beneficial for preserving the precursor morphology/structure in MOF-derived carbon materials.
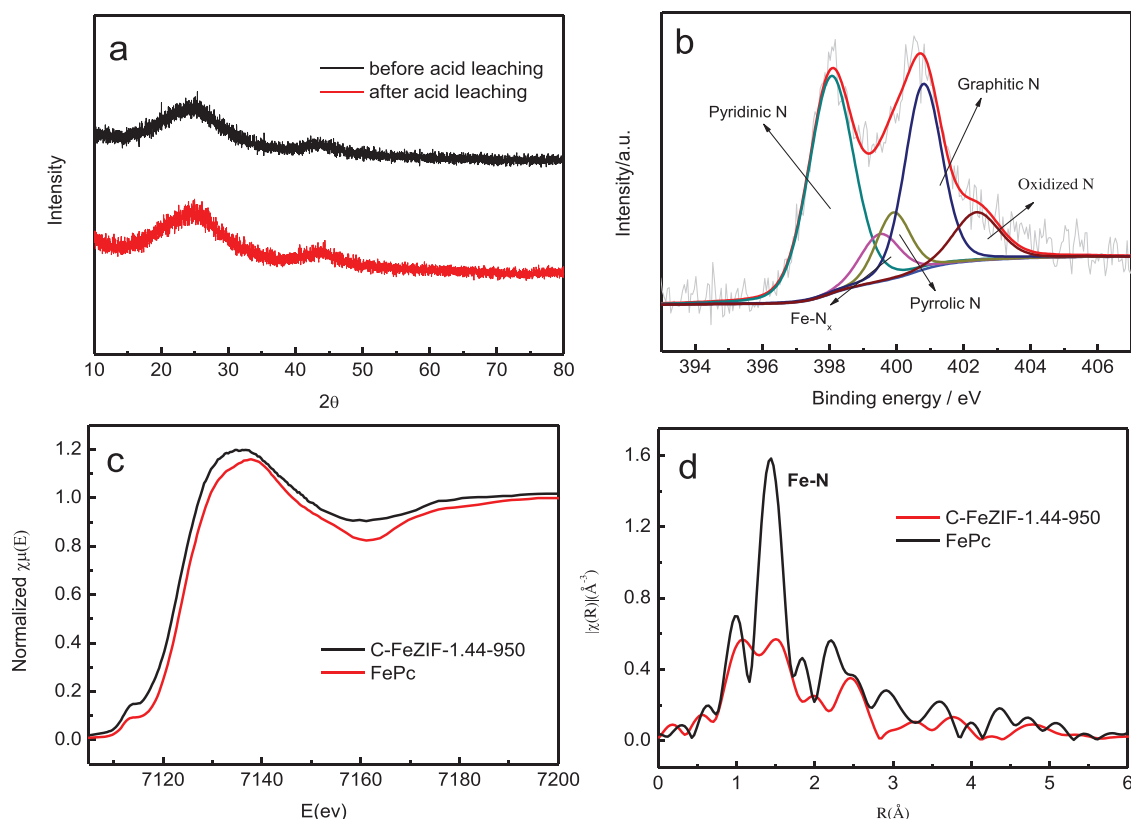
ADVANCED
SCIENCE NEWS
www.advancedsciencenews.com

ADVANCED
ENERGY
MATERIALS
www.advenergymat.de
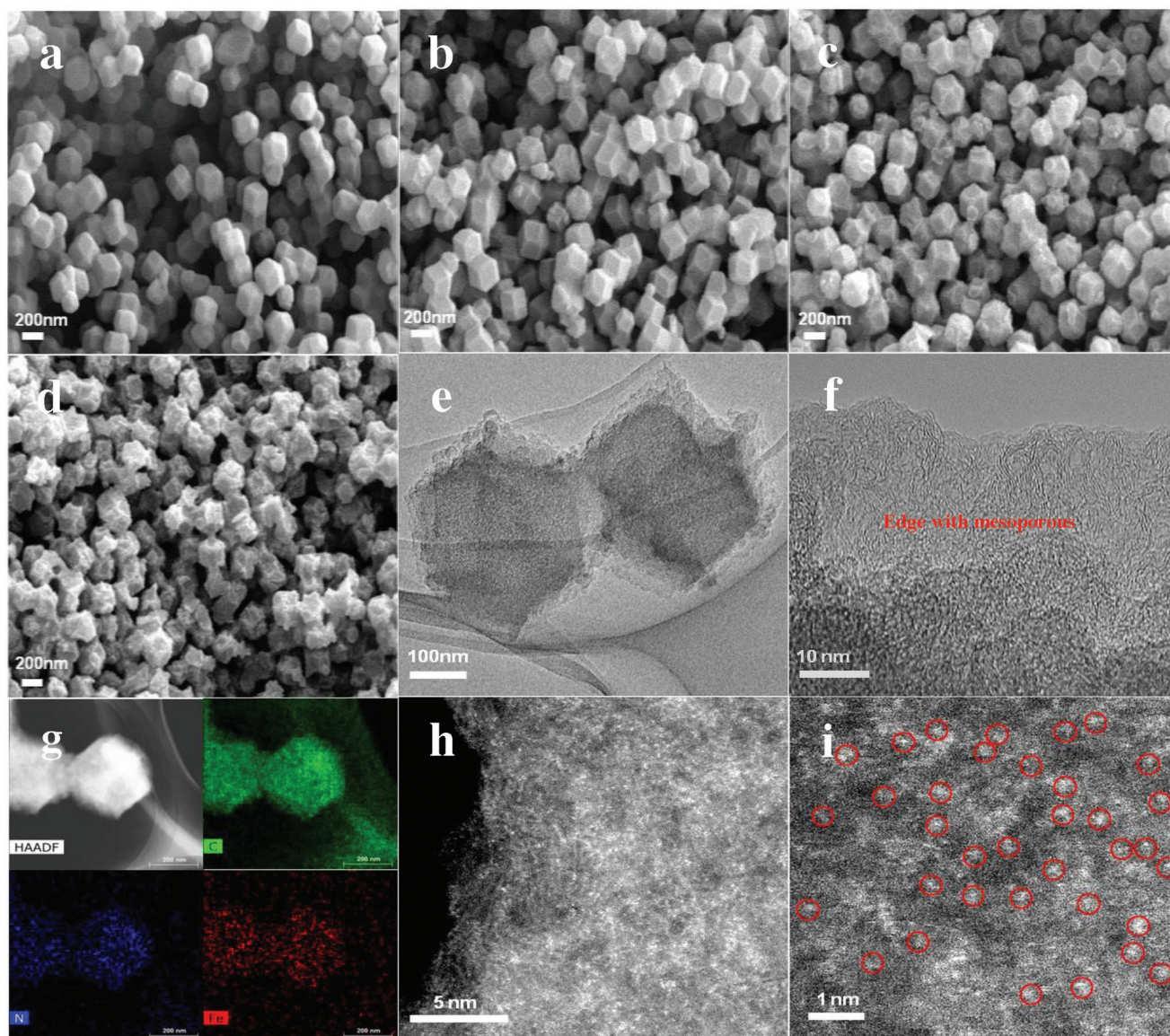
Figure 1. SEM images of a) C-ZIF-8-950, b) C-FeZIF-0.22-950, c) C-FeZIF-1.44-950, and d) C-FeZIF-4.44-950; e,f) TEM images of C-FeZIF-1.44-950 at different magnifications; g) elemental mapping of C-FeZIF-1.44-950; h) AC HAADF-STEM image of C-FeZIF-1.44-950 and i) enlargement of image in h).

Figure 1e,f shows the HRTEM images of C-FeZIF-1.44-950 (our optimal sample, based on ORR performance; please see Figure 3). The HRTEM image (Figure 1e) also reveals the material's well-defined polyhedral shape and highly porous character. The surface of the carbon polyhedrons in C-FeZIF-1.44-950 (see Figure 1f) became rough, and a mesoporous graphene-like structure at the edges could be clearly observed, comparable to the microporous carbon polyhedron derived from carbonized ZIF-8 (Figure S2a, Supporting Information). The abundant defects and edge sites as well as favorable mesoporosity (Figure 1f) could greatly promote the ORR. More importantly, no Fe species particles are observable in the TEM images of C-FeZIF-1.44-950, suggesting that the Fe may have been homogeneously dispersed and coordinated with N atoms in the carbon nanoframes by our gaseous doping process. Elemental mapping of C-FeZIF-1.44-950

(see Figure 1g) further revealed that Fe and N were highly dispersed and well distributed in the carbon framework.

The AC HAADF-STEM images in Figure 1h,i suggest that the Fe was dispersed at the atomic scale; a large number of bright dots (iron atoms) are clearly observable, but no clusters or small particles of Fe-associated species.[14]

The surface area of C-FeZIF-1.44-950 reached 1255 m^2 g^{-1}, and typical Type IV isotherm characteristics isotherm with hysteresis loops in the medium pressure regions($P/P_o = 0.5–0.7$) were observed(see Figure S4, Supporting Information), demonstrating a micro-mesoporous hierarchical porous structure existed in the sample. This suggested the addition of ferrocene introduced a mesoporous structure into the carbon polyhedral, different from the predominant microporous characteristics of C-ZIF-8-950 without Fe doping (see Figure S4, Supporting Information); this further demonstrates the advantages of our

**ADVANCED
SCIENCE NEWS**
www.advancedsciencenews.com

**ADVANCED
ENERGY
MATERIALS**
www.advenergymat.de

Figure 2. a) XRD patterns of C-FeZIF-1.44-950 before and after acid leaching; b) XPS spectrum of N 1s in C-FeZIF-1.44-950; c) Fe K-edge XANES spectra and d) FT-EXAFS spectra of C-FeZIF-1.44-950 and FePc.

metalorganic gaseous doping approach, which easily yielded a derived carbon material with single Fe doping, a well-preserved morphology, a balanced porous structure, and high surface area. All of these features would facilitate mass transfer, increase active-site exposure, and contribute to high ORR performance.[27,28]
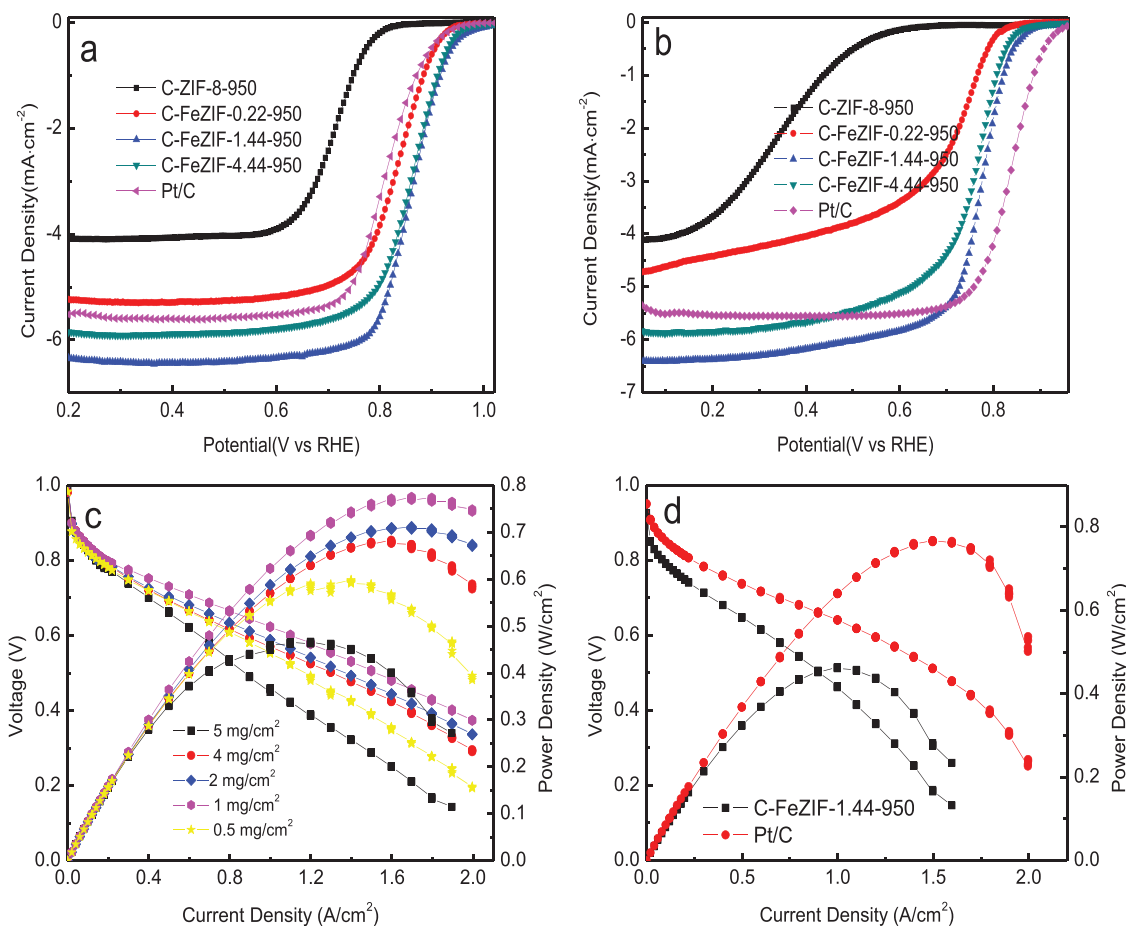
Figure 2a shows the XRD patterns of C-FeZIF-1.44-950 before and after acid leaching. The patterns' shapes are almost the same, exhibiting broad diffraction peaks at 20°–30° and 40°–50°, assignable to the (002) and (101) crystal faces of graphitic carbon. It should be pointed out that prior to acid leaching, no peaks associated with iron oxides, Fe, or iron carbides were observed, further confirming that all of the Fe atoms may have been atomically incorporated into the carbon framework by our approach. These results are consistent with those obtained by STEM analysis.[8,9]

With X-ray photoelectron spectroscopy (XPS), we determined that the N content of C-FeZIF-1.44-950 reached 5.51 at%, and the Fe content was 1 wt% (Figure S5, Supporting Information). Evidently, the gaseous doping of Fe with ferrocene as the precursor significantly reduced the content of oxidized N, induced the formation of Fe–N_x, and increased the fraction of graphitic-N in comparison to C-ZIF-8-950 (without ferrocene doping).

To gain insight into the status of Fe, X-ray absorption spectroscopy (XAS) was employed to investigate electronic and coordination information for Fe-involved species in C-FeZIF-1.44-950. As shown in Figure 2c,d, the Fe K-edge XANES spectrum of C-FeZIF-1.44-950 was similar to that of FePc, implying that the Fe single atoms may have carried positive charges and could have been stabilized by N atoms.[19] The fingerprint peak at ≈7113 eV demonstrates the existence of the square-planar Fe–N_4 species in C-FeZIF-1.44-950.[29] The Fourier transform extended X-ray absorption fine structure (FT-EXAFS) spectrum at the Fe K-edge shows a strong peak at about 1.5 Å, attributable to Fe–N scattering paths. No Fe—Fe bond at about 2.1 Å can be detected, suggesting that the Fe dopant was distributed in the carbon framework exclusively as single Fe atoms. This would indicate that our novel ferrocene gaseous doping process promoted the formation of isolated Fe atoms, resulting in the atomic dispersion of Fe and a high content of Fe-N_4 coordination, which would contribute to the catalyst's high performance.[8,14]

Based on the Brunauer–Emmett–Teller (BET) specific surface area, XPS, and XAS analysis results, we first calculated the active-site density of the sample. The density of active Fe atoms (or Fe–N_x active sites) reached 1.75812×10^{13} sites cm^{-2} (2.20644×10^{20} sites per gram of catalyst), and the density of active N (the number of nitrogen active sites per square centimeter) was 1.93693×10^{14} sites cm^{-2}, confirming the high densities of active N and active Fe in our C-FeZIF-1.44-950, prepared with our gaseous doping approach. We cannot compare these values with earlier data because as far as we know no such calculations have previously been reported. The active N and active Fe densities of our C-FeZIF-1.44-950 are further higher than those of samples prepared by our group with a conventional doping method.

ADVANCED
SCIENCE NEWS
www.advancedsciencenews.com

ADVANCED
ENERGY
MATERIALS
www.advenergymat.de

Figure 3. LSV curves of C-ZIF-8-950, C-FeZIF-0.22-950, C-FeZIF-1.44-950, C-FeZIF-4.44-950, and 20 wt% Pt/C in O_2-saturated 0.1 M KOH a) and 0.1 M HClO$_4$ b) (rotation rate: 1600 rpm). Polarization curves and power density plots with C-FeZIF-1.44-950 as the cathode catalyst for a H_2/O_2 PEMFC c) and a H_2/air PEMFC d) with C-FeZIF-1.44-950 (1 mg cm^{-2}) or commercial Pt/C (0.2 mg cm^{-2}) as the cathode catalyst.
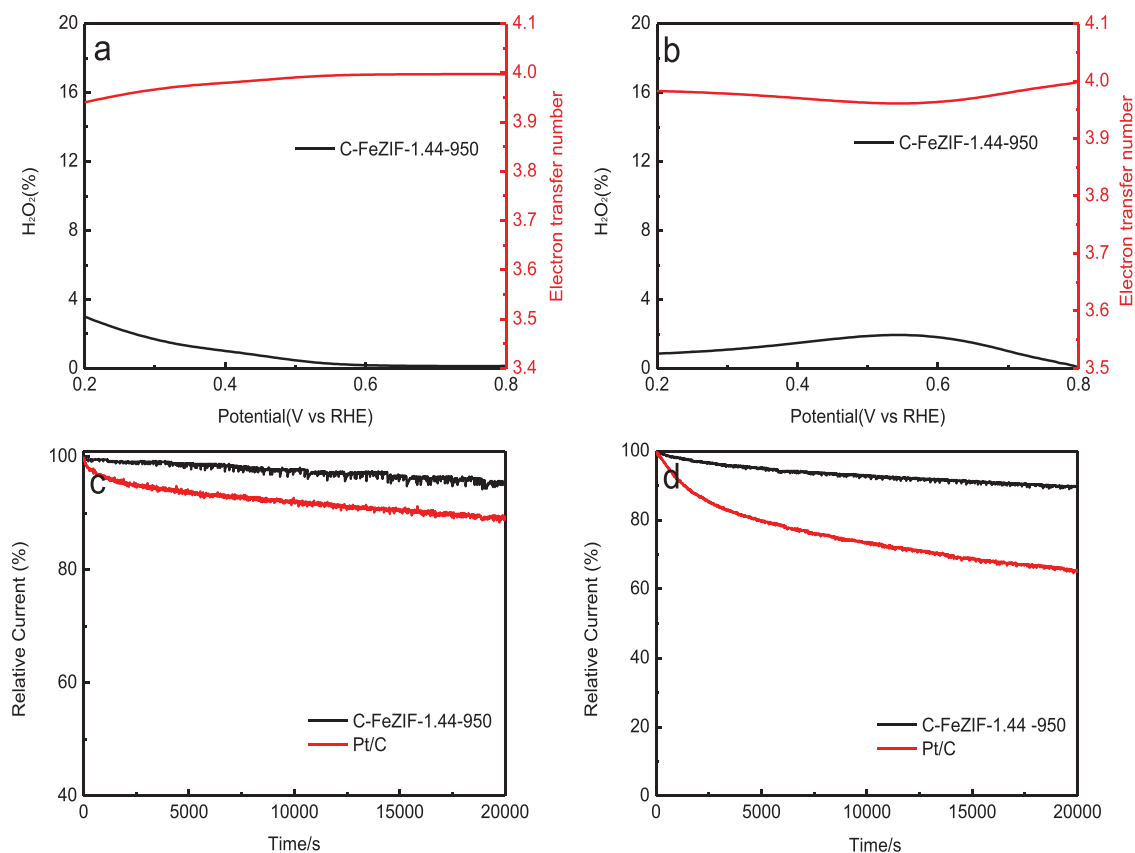
Figure 3 shows the ORR polarization curves of the catalysts in O_2-saturated 0.1 M KOH and 0.1 M HClO$_4$ solutions. As expected, Fe doping greatly improved the ORR performance in both alkaline and acidic media, especially in the latter. The sample with a ferrocene to ZIF-8 ratio of 1.44, C-FeZIF-1.44-950, exhibited the best ORR performance in both media. In 0.1 M KOH, the half-wave potential reached 0.864 V, 50 mV higher than that of commercial Pt/C; in 0.1 M HClO$_4$ solution, its half-wave potential was 0.78 V, only 60 mV less than that of Pt/C catalyst. To the best of our knowledge, C-FeZIF-1.44-950 is currently one of the best nonplatinum carbon catalysts for the ORR (see Tables S1 and S2, Supporting Information).

It is encouraging that C-FeZIF-1.44-950 exhibited excellent cathodic ORR performance in H_2/O_2 and H_2/air fuel cell systems (see Figure 3c,d). The optimal loading of our C-FeZIF-1.44-950 could be lower to 1 mg cm^{-2}, which is much lower than conventional used loading of 4 mg cm^{-2}. At meaningful working voltage in view of energy efficiency, an optimized membrane electrode assembly (MEA) with 1 mg cm^{-2} catalyst loading at the cathode yielded a maximum power density of 775 W cm^{-2}, while the current density reached 1100 mA cm^{-2} at 0.6 V and 637 mA cm^{-2} at 0.7 V. This is a remarkable result, surpassing most previously reported figures (Table S3, Supporting

Information). Furthermore, effects temperature and back pressure on performance of fuel cell were investigated, and shown in Figure S7 in the Supporting Information. We ascribe the high performance in both an RDE and a PEMFC to the catalyst's single Fe atom doping and high density of Fe–N$_x$ active sites, which produced sufficient activity with a thin catalyst layer, promoting management of water and heat for the fuel cell.

When we investigated the MEA's performance in a single-cell system fed with air instead of oxygen, we again found that it exhibited excellent performance. As shown in Figure 3d, the current density was 650 mA cm^{-2} at 0.6 V and 350 mA cm^{-2} at 0.7 V, and the maximum power density was 463 mW cm^{-2}. As far as we know, this outperforms most performance data reported for a single fuel cell with doped carbon as the cathode catalyst operated in a H_2/air flow; we present the recently reported data in Table S4 in the Supporting Information.

To understand the catalyst's high performance, we conducted rotating ring-disk electrode analysis to investigate the catalyst's selectivity for the four-electron ORR. **Figure 4**a,b shows electron transfer values (*n*) for C-FeZIF-1.44-950 of 3.98 in 0.1 M KOH and 3.97 in 0.1 M HClO$_4$. C-FeZIF-1.44-950 generated negligible H_2O_2 yields of below 4% and 2%, respectively, during the ORR, demonstrating a high selectivity for a four-electron process in

**ADVANCED
SCIENCE NEWS**

www.advancedsciencenews.com

**ADVANCED
ENERGY
MATERIALS**

www.advenergymat.de

Figure 4. Peroxide yield and electron transfer number (n) of C-FeZIF-1.44-950 in O_2-saturated a) 0.1 M KOH and b) 0.1 M $HClO_4$; long-term durability measurements of C-FeZIF-1.44-950 and Pt/C for 20 000 s in O_2-saturated c) 0.1 M KOH and d) 0.1 M $HClO_4$.

both electrolytes. C-FeZIF-1.44-950 also exhibited excellent stability in both alkaline and acid media. In 0.1 M KOH, it retained more than 96% of its relative current after continuous operation for 20 000 s, compared to an 11% loss with commercial Pt/C; in 0.1 M $HClO_4$ solution, it also retained more than 90% of its initial ORR performance after 20 000 s, which was much better than Pt/C (65%). We also investigated the long-term stability of C-FeZIF-1.44-950 in a H_2/air PEMFC using constant-current operation testing at 1000 mA cm^{-2}. The working voltage loss was only 32.2% after 10 h (Figure S8, Supporting Information). It is worth pointing out that the durability of our catalyst in a single PEMFC outperformed most reported Fe–N_x/C electrocatalysts,[30–32] although it still falls short of requirements for application in the automotive industry.

In summary, a high-performance doped-carbon catalyst with high-density active sites was successfully prepared using a metalorganic gaseous doping method, with ferrocene as the Fe precursor and ZIF-8 as the host. The catalyst retained the morphology of ZIF-8, and the iron was highly dispersed in the catalyst as single Fe atoms coordinated with N to form Fe–N_x active sites. The catalyst not only exhibited excellent ORR activity and stability towards oxygen reduction in both acidic and alkaline media but also presented superb single-cell PEMFC performance. Our work demonstrates the feasibility of using a doped-carbon catalyst instead of Pt/C as the cathode in a PEMFC to achieve comparable performance, although our catalyst's durability still needs improvement.

Experimental Section

Electrocatalyst Preparation: Synthesis of ZIF-8 Nanocrystals: ZIF-8 was synthesized following a method described in the literature.[23] Typically, 2-methylimidazole with a mass of 3 g was added into 20 mL methanol, 10 mL methanol containing 0.8 g Zn$(NO_3)_2 \cdot 6H_2O$ was poured into the above solution with stirring for 24 h at room temperature. The product was separated by centrifugation and washed with methanol, and dried.

Preparation of Catalysts: In a typical procedure, 0.45 g ZIF-8 and 0.65 g ferrocene were individually placed in a porcelain boat (see Scheme 1). The boat was heated under an Ar atmosphere to 150 °C at a rate of 2 °C min^{-1}, then kept at that temperature for 2 h. The temperature was further increased to 950 °C at a rate of 5 °C min^{-1}, held there for 3 h for pyrolysis, then cooled down to room temperature. The resulting black powder was leached with 0.5 M H_2SO_4 at 80 °C for 12 h, followed by washing with DI water and annealing at 950 °C again for further graphitization. Ferrocene, the vaporable Fe precursor, was vaporized into gas molecules during low temperature, then the ferrocene molecules were diffused into the ZIF-8 sample under an Ar flow. Analysis of the Fe content showed that only a small amount of the ferrocene was trapped by the ZIF-8, while the rest was removed in the Ar flow. Nonetheless, the recipe mass ratio of ferrocene to ZIF-8 still significantly affected the performance of the final prepared catalysts.

The prepared catalysts are denoted as C-FeZIF-X-950, where "X" indicates the recipe mass ratio of ferrocene to ZIF-8.

Materials Characterization: All samples were characterized using the following equipment: Merlin field emission scanning electron microscope (Carl Zeiss); JEM-2100 transmission electron microscope (JEOL, Japan) operating at 120 kV; TD-3500 powder diffractometer (Tongda, China) operating at 30 kV and 20 mA; VG ESCALAB MK2 X-ray photoelectron spectrometer (VG Corporation, UK) using an Al-Kα X-ray

source; and Tristar 3020 gas adsorption analyzer (Micromeritics, USA) at 77 K to determine BET surface area and pore distribution.

XAS measurement on Fe K-edge was performed using the SXRMB beam line of Canadian Light Source. The SXRMB beamline used an Si(111) double crystal monochromator to cover an energy range of 2–10 keV with a resolving power of 10 000. A four-element Si(Li) drift detector was used to record the fluorescence spectrum in a vacuum chamber. The powder sample was spread onto double sided, conducting carbon tape. Fe foil was used to calibrate the beam line energy. The XAS results were analyzed using Athena program.

Electrocatalytic Testing: All electrochemical measurements were conducted on an Ivium electrochemical workstation (Ivium, Netherlands) in a standard three-electrode system. The reference electrode was Ag/AgCl in the acidic medium and Hg/HgO in the alkaline medium. A Pt wire was using as the counter electrode; and a glassy carbon electrode (GC, 0.196 cm^2) was using as the working electrode. 5 mg catalysts are dispersed by sonication in 1 mL Nafion/ethanol (0.25 wt% Nafion). Then 20 μL catalysts ink was covered on glassy carbon electrode and dried. In the end, the catalyst loading was about 0.5 mg cm^{-2}.

In this work, the ORR polarization curves linear sweep voltammetry (LSV) and cyclic voltammograms of all catalysts were obtained at a scan rate of 10 mV s^{-1} in O$_2$- or N$_2$- saturated 0.1 M KOH or 0.1 M HClO$_4$ solution.

The hydrogen peroxide yield (H$_2$O$_2$%) and the electron transfer number (N) were calculated using the following equations:

$$\eta = 200 I_r \left(N I_d + I_r \right)^{-1}$$

$$n = 4 I_d (I_d + I_r N^{-1})^{-1}$$

Here, I_d and I_r represent disk and ring current, respectively, and N is the ring collection efficiency.

To investigate the catalysts' durability, the chronoamperometry was conducted at 0.65 V for 20 000 s (900 rpm) in O$_2$-saturated 0.1 M KOH and 0.62 V for 20 000 s (900 rpm) in an O$_2$-saturated 0.1 M HClO$_4$ solution.

MEA Testing: The MEA for an H$_2$/O$_2$ PEM fuel cell was prepared using a catalyst-sprayed membrane method reported previously by our group and conducted in an Arbin fuel cell testing system (Arbin, USA). In a typical approach, the catalyst "ink" was sprayed on one side of a Nafion 211 membrane (DuPont, USA) in order to form the cathode catalyst layer, and a commercial JM Pt/C catalyst was used at the anode. The active area of the MEA was 5.0 cm^2. The Fe–N$_x$/C catalyst loadings at the cathode were 0.5–5 mg cm^{-2}, and the Pt loadings at the anode was 0.1 mg cm^{-2}. The Nafion content in the catalyst layer was about 50 wt%. H$_2$ and O$_2$/air as the fuel and oxidant were fed with full humidification at 30 psi back pressure and a flow rate of 300 mL min^{-1}, and the cell testing temperature was 80 °C.

Supporting Information

Supporting Information is available from the Wiley Online Library or from the author.

Acknowledgements

Conflict of Interest

The authors declare no conflict of interest.

[1] Y. Nie, L. Li, Z. Wei, *Chem. Soc. Rev.* **2015**, *44*, 2168.
[2] J. K. Dombrovskis, A. E. C. Palmqvist, *Fuel Cells* **2016**, *16*, 4.
[3] M. Shao, Q. Chang, J.-P. Dodelet, R. Chenitz, *Chem. Rev.* **2016**, *116*, 3594.
[4] T. Sun, B. Tian, J. Lu, C. Su, *J. Mater. Chem. A* **2017**, *5*, 18933.
[5] J. Zhang, L. Dai, *ACS Catal.* **2015**, *5*, 7244.
[6] K. Strickland, E. Miner, Q. Jia, U. Tylus, N. Ramaswamy, W. Liang, M.-T. Sougrati, F. Jaouen, S. Mukerjee, *Nat. Commun.* **2015**, *6*, 7343.
[7] Y. J. Sa, D.-J. Seo, J. Woo, J. T. Lim, J. Y. Cheon, S. Y. Yang, J. M. Lee, D. Kang, T. J. Shin, H. S. Shin, H. Y. Jeong, C. S. Kim, M. G. Kim, T.-Y. Kim, S. H. Joo, *J. Am. Chem. Soc.* **2016**, *138*, 15046.
[8] P. Chen, T. Zhou, L. Xing, K. Xu, Y. Tong, H. Xie, L. Zhang, W. Yan, W. Chu, C. Wu, Y. Xie, *Angew. Chem., Int. Ed.* **2017**, *56*, 610.
[9] Q.-L. Zhu, W. Xia, L.-R. Zheng, R. Zou, Z. Liu, Q. Xu, *ACS Energy Lett.* **2017**, *2*, 504.
[10] H. Zhang, S. Hwang, M. Wang, Z. Feng, S. Karakalos, L. Luo, Z. Qiao, X. Xie, C. Wang, D. Su, Y. Shao, G. Wu, *J. Am. Chem. Soc.* **2017**, *139*, 14143.
[11] W. Zhang, X. Xu, C. Zhang, Z. Yu, Y. Zhou, Y. Tang, P. Wu, S. Guo, *Small Methods* **2017**, *1*, 1700167.
[12] J. Wang, Z. Huang, W. Liu, C. Chang, H. Tang, Z. Li, W. Chen, C. Jia, T. Yao, S. Wei, Y. Wu, Y. Li, *J. Am. Chem. Soc.* **2017**, *139*, 17281.
[13] J.-C. Li, Z.-Q. Yang, D.-M. Tang, L. Zhang, P.-X. Hou, S.-Y. Zhao, C. Liu, M. Cheng, G.-X. Li, F. Zhang, H.-M. Cheng, *NPG Asia Mater.* **2018**, *10*, e461.
[14] Y. Chen, S. Ji, Y. Wang, J. Dong, W. Chen, Z. Li, R. Shen, L. Zheng, Z. Zhuang, D. Wang, Y. Li, *Angew. Chem., Int. Ed.* **2017**, *56*, 6937.
[15] Q. Li, W. Chen, H. Xiao, Y. Gong, Z. Li, L. Zheng, X. Zheng, W. Yan, W. Cheong, R. Shen, N. Fu, L. Gu, Z. Zhuang, C. Chen, D. Wang, Q. Peng, J. Li, Y. Li, *Adv. Mater.* **2018**, *30*, 1800588.
[16] K. Shen, X. Chen, J. Chen, Y. Li, *ACS Catal.* **2016**, *6*, 5887.
[17] H. Zhang, H. Osgood, X. Xie, Y. Shao, G. Wu, *Nano Energy* **2017**, *31*, 331.
[18] L. Liu, A. Corma, *Chem. Rev.* **2018**, *118*, 4981.
[19] L. Jiao, G. Wan, R. Zhang, H. Zhou, S.-H. Yu, H.-L. Jiang, *Angew. Chem.* **2018**, *130*, 8661.
[20] J. Wang, G. Han, L. Wang, L. Du, G. Chen, Y. Gao, Y. Ma, C. Du, X. Cheng, P. Zuo, G. Yin, *Small* **2018**, *14*, 1704282.
[21] F. Jaouen, E. Proietti, M. Lefèvre, R. Chenitz, J.-P. Dodelet, G. Wu, H. T. Chung, C. M. Johnston, P. Zelenay, *Energy Environ. Sci.* **2011**, *4*, 114.
[22] X. X. Wang, D. A. Cullen, Y.-T. Pan, S. Hwang, M. Wang, Z. Feng, J. Wang, M. H. Engelhard, H. Zhang, Y. He, Y. Shao, D. Su, K. L. More, J. S. Spendelow, G. Wu, *Adv. Mater.* **2018**, *30*, 1706758.
[23] Y. Deng, Y. Dong, G. Wang, K. Sun, X. Shi, L. Zheng, X. Li, S. Liao, *ACS Appl. Mater. Interfaces* **2017**, *9*, 9699.
[24] Z. Liu, F. Sun, L. Gu, G. Chen, T. Shang, J. Liu, Z. Le, X. Li, H. Wu, Y. Lu, *Adv. Energy Mater.* **2017**, *7*, 1701154.
[25] Z. Mo, S. Liao, Y. Zheng, Z. Fu, *Carbon* **2012**, *50*, 2620.
[26] Y. Qu, Z. Li, W. Chen, Y. Lin, T. Yuan, Z. Yang, C. Zhao, J. Wang, C. Zhao, X. Wang, F. Zhou, Z. Zhuang, Y. Wu, Y. Li, *Nat. Catal.* **2018**, *1*, 781.
[27] M. Xiao, J. Zhu, L. Feng, C. Liu, W. Xing, *Adv. Mater.* **2015**, *27*, 2521.

[28] Z. Zhang, X. Gao, M. Dou, J. Ji, F. Wang, *J. Mater. Chem. A* **2017**, *5*, 1526.

[29] Q. Lai, L. Zheng, Y. Liang, J. He, J. Zhao, J. Chen, *ACS Catal.* **2017**, *7*, 1655.

[30] Q. Liu, X. Liu, L. Zheng, J. Shui, *Angew. Chem.* **2018**, *130*, 1218.

[31] Y.-C. Wang, Y.-J. Lai, L. Song, Z.-Y. Zhou, J.-G. Liu, Q. Wang, X.-D. Yang, C. Chen, W. Shi, Y.-P. Zheng, M. Rauf, S.-G. Sun, *Angew. Chem.* **2015**, *127*, 10045.

[32] A. Zitolo, V. Goellner, V. Armel, M.-T. Sougrati, T. Mineva, L. Stievano, E. Fonda, F. Jaouen, *Nat. Mater.* **2015**, *14*, 937.